Article

Real-Time Estimation of BDS-3 Satellite Clock Offset with Ambiguity Resolution Using B1C/B2a Signals

Wei Xie [1,2], Kan Wang [1,2,3,*], Wenju Fu [4], Shichao Xie [5], Bobin Cui [5] and Mengyuan Li [5]

1   National Time Service Center, Chinese Academy of Sciences, Xi'an 710600, China; xiewei@ntsc.ac.cn
2   Key Laboratory of Time Reference and Applications, Chinese Academy of Sciences, Xi'an 710600, China
3   University of Chinese Academy of Sciences, Beijing 100049, China
4   State Key Laboratory of Information Engineering in Surveying, Mapping and Remote Sensing,
     Wuhan University, Wuhan 430079, China; wenjufu@whu.edu.cn
5   College of Geology Engineering and Geomatics, Chang'an University, Xi'an 710054, China;
     wonderwall@chd.edu.cn (S.X.); bobin@chd.edu.cn (B.C.); limengyuan@chd.edu.cn (M.L.)
*   Correspondence: wangkan@ntsc.ac.cn

Abstract: The third generation of the BeiDou navigation satellite system (BDS-3) can transmit five-frequency signals. The real-time satellite clock offset of BDS-3 is typically generated utilizing the B1I/B3I combination with the ambiguity-float solutions. By conducting the ambiguity resolution (AR), the reliability of the satellite clock offset can be improved. However, the performance of BDS-3 ambiguity-fixed real-time satellite clock offset with B1C/B2a signals remains unknown and unrevealed. In this contribution, the performance of the BDS-3 ambiguity-fixed satellite clock offset with the new B1C/B2a signals is investigated. One week of observation data from 85 stations was used to perform ambiguity-fixed satellite clock offset estimation. For B1I/B3I and B1C/B2a signals, the wide-lane (WL) uncalibrated phase delay (UPD) on the satellite end is fairly stable for one day, while the narrow-lane (NL) UPD standard deviation (STD) amounts to 0.122 and 0.081 cycles, respectively. The mean ambiguity fixing rate is 80.7% and 78.0% for these two signal combinations, and the time to first fix (TTFF) for the B1C/B2a signals is remarkably shorter than that of the B1I/B3I signals. The STDs of the ambiguity-float and -fixed satellite clock offsets are 0.033 and 0.026 ns, respectively, for the B1I/B3I combination, and it is reduced to 0.024 and 0.023 ns for B1C/B2a signals, respectively. Using the estimated UPD and clock offset products, the positioning performance of the kinematic Precise Point Positioning (PPP)-AR results amounts to 1.56, 1.23, and 4.46 cm in the east, north, and up directions for B1I/B3I signals, respectively. It is improved to 1.36, 1.16, and 4.25 cm using the products estimated with the B1C/B2a signals, with improvements of 12.8%, 5.7%, and 4.7% in three directions, respectively. The experiments showed that the performances of the ambiguity-fixed satellite clock offsets and the PPP-AR results using B1C/B2a signals are better than those of B1I/B3I.

Keywords: BDS-3; satellite clock offset estimation; AR; B1C/B2a; PPP-AR

1. Introduction

The third generation of the BeiDou satellite navigation system (BDS-3) was completed on 31 July 2020 and consists of 27 satellites with heterogeneous constellations. Different from BDS-1 and BDS-2, the BDS-3 can transmit signals on more frequency bands, and it can nowadays provide more services, like basic navigation, Satellite-Based Augmentation System (SBAS), short message communication, and Precise Point Positioning (PPP) services [1].

To achieve PPP, the satellite clock offset is significantly essential, which is also the foundation for satellite clock performance monitoring. Since the onboard satellite clocks are sensitive to the space environment and other factors, the long-term clock offset prediction is challenged [2,3]; therefore, to obtain high-precision real-time satellite clocks, one usually

estimates it in real-time with a high frequency. The BDS-3 satellite clock offset is usually obtained using the Ionospheric-Free (IF) combination on B1I and B3I frequency bands. However, BDS-3 can also transmit on other frequency bands, such as B1C, B2a, and B2b.

The difference between the BDS-3 legacy and the new signals is the signal frequency, structure, modulation techniques, and bandwidth [4–8], and many studies have been conducted on the new signals. For example, in terms of the service end, different signal combinations are used to determine precise satellite orbits. The orbital overlapping Root Mean Squares (RMS) using the B1C/B2a combination shows a better performance [9]. The satellite antenna Phase Center Offset (PCO) and Variation (PCV) model on BDS-3 B1C/B2a signals is proposed, with the detailed PCO and PCV values given [10]. The multi-frequency uncombined satellite clock offset is investigated, where its accuracy is about 0.03 ns [11]. For the user end, the quality of observation on five-frequency BDS-3 was evaluated, in which it was found that the B1C/B2a code and carrier phase signal strengths showed superior performance [12]. The B1C/B2a signals were also applied to determine the Haiyang-2D satellite orbit, where the orbit accuracy is 2.3 cm [13]. The BDS-3 SBAS corrections were generated using the B1C/B2a signals, with clock corrections only, and the 95% percentile line of the positioning errors was reduced by about 48% compared to the case without SBAS corrections [14]. The observable-specific phase bias products using B1C/B2a were estimated and applied to kinematic PPP ambiguity resolution (AR), and centimeter-level positioning accuracy can be achieved [15]. The BDS-3 wide-area positioning performance was investigated, which demonstrated that the PPP convergence time using B1C/B2a signals was significantly shortened compared to the B1I/B3I signals [16]. The PPP time transfer was also investigated using the B1C/B2a signals, and the time links using B1C/B2a signals were shown to be more stable [17]. The BDS-3 new signals have been used in diverse precise data processing applications. Although the AR technology can improve the estimated satellite clock offset performance [18], the legacy B1I/B3I signals were used in previous studies. Considering that the signal frequency, structure, modulation techniques, and bandwidth are different for the B1I/B3I and B1C/B2a combination, we evaluated and compared the performance of BDS-3 ambiguity-fixed real-time satellite clock offset between the legacy B1I/B3I and new B1C/B2a signals.

This contribution focuses on the BDS-3 ambiguity-fixed real-time satellite clock offset estimation using the new B1C/B2a signals. Observations from the Multi-GNSS Experiment (MGEX) [19] project are applied to the experiments. After the introduction, the model of ambiguity-float BDS-3 satellite clock estimation, uncalibrated phase delay (UPD) estimation, and the AR strategies are presented. Afterward, the experiments are described, and the clock offset performance is evaluated from the following aspects: the UPD performance, the ambiguity fixing rate, the clock offset accuracy, and the kinematic PPP-AR. The performances of the estimated clock offset using B1C/B2a and legacy B1I/B3I signals are then compared. The conclusion is given at the end.

2. Methods

The mathematical model for ambiguity-float satellite clock offset estimation is given first. The strategies for the UPD estimation and AR are described next. Thereafter, the data processing is introduced in detail.

2.1. Model for Ambiguity-Float Satellite Clock Offset Estimation

The IF combination on dual-frequency observations is applied to generate a precise satellite clock offset:

$$P_{r,IF}^s = \rho_r^s + c(t_{r,IF} - t_{IF}^s) + T_r^s + \varepsilon_{r,pc}^s \tag{1}$$

$$L_{r,IF}^s = \rho_r^s + c(t_{r,IF} - t_{IF}^s) + \lambda_{IF} N_{r,IF}^s + T_r^s + e_{r,lc}^s \tag{2}$$

where s and r are the satellite and receiver, respectively. $P_{r,IF}^s$ and $L_{r,IF}^s$ represent code and carrier phase dual-frequency IF observations, respectively. ρ_r^s is the geometric distance. c denotes the speed of light. $t_{r,IF}$ and t_{IF}^s represent the receiver and satellite clock offsets

containing corresponding IF code hardware biases with the unit of second, respectively. T_r^s is slant tropospheric delay. λ_{IF} is the wavelength of the IF combination. $N_{r,IF}^s$ is IF ambiguity [20]. $\varepsilon_{r,pc}^s$ and $e_{r,lc}^s$ are unmodeled errors for code and phase observations, respectively. Moreover, other errors, like the receiver and satellite PCOs and PCVs, phase wind-ups, relativistic effect, and station displacement are carefully considered in Equations (1) and (2). Then, the observation equation can be transferred into error equations:

$$v_{r,pc}^s = c\left(\bar{t}_{r,IF} - \bar{t}_{IF}^s\right) + m_r^s \overline{Z}_r - l_{r,pc}^s \tag{3}$$

$$v_{r,lc}^s = c\left(\bar{t}_{r,IF} - \bar{t}_{IF}^s\right) + \lambda_{IF}\overline{N}_{r,IF}^s + m_r^s \overline{Z}_r - l_{r,pc}^s \tag{4}$$

where $v_{r,pc}^s$ and $v_{r,lc}^s$ are the a posteriori residuals for code and carrier observations, respectively. m_r^s is the tropospheric mapping function. $l_{r,pc}^s$ and $l_{r,lc}^s$ represent the code and phase a priori residuals, respectively. $\bar{t}_{r,IF}$, $\bar{t}_{IF}^s$, $\overline{Z}_r$, and $\overline{N}_{r,IF}^s$ are the estimable parameters, in which the $\overline{Z}_r$ is zenith wet delay (ZWD). Then, by combining the observations from globally distributed stations, the error equations can be expressed as a matrix form [21]:

$$V = A_1 X_1 + A_2 X_2 - L, \ P \tag{5}$$

where V is the a posteriori residuals vector, and A_1 is the coefficients of active parameters, i.e., satellite clock offset and receiver clock offset. A_2 are coefficients for inactive parameters, which are tropospheric ZWD and ambiguity. X_1 and X_2 are the estimated parameters. L is the a priori residuals vector. P is the elevation-related weight matrix.

Next, the sequential least-square adjustment [21] is applied to estimate parameters. The normal equation can be expressed as follows:

$$\begin{bmatrix} N_{11} & N_{12} \\ N_{21} & N_{22} \end{bmatrix} \begin{bmatrix} X_1 \\ X_2 \end{bmatrix} = \begin{bmatrix} W_1 \\ W_2 \end{bmatrix} \tag{6}$$

where $N_{11} = A_1^T P A_1$, $N_{12} = A_1^T P A_2$, $N_{21} = N_{12}^T$, $N_{22} = A_2^T P A_2$, $W_1 = A_1^T P L$, $W_2 = A_2^T P L$. Equation (6) can be re-formulated as follows after simplification:

$$\begin{bmatrix} N_{11} & N_{12} \\ 0 & N_2 \end{bmatrix} \begin{bmatrix} X_1 \\ X_2 \end{bmatrix} = \begin{bmatrix} W_1 \\ R_2 \end{bmatrix} \tag{7}$$

where $N_2 = N_{22} - N_{21}N_{11}^{-1}N_{12}$, $R_2 = W_2 - N_{21}N_{11}^{-1}W_1$. For the first epoch, the least-square adjustment is used:

$$\begin{bmatrix} X_1 \\ X_2 \end{bmatrix} = \begin{bmatrix} N_{11} & N_{12} \\ 0 & N_2 \end{bmatrix}^{-1} \begin{bmatrix} W_1 \\ R_2 \end{bmatrix} \tag{8}$$

For the i-th ($i > 1$) epoch, the normal equation can be expressed as follows:

$$\begin{bmatrix} N_{11} & N_{12} \\ 0 & N_{2(1)} + N_{2(2)} + \ldots + N_{2(i)} \end{bmatrix} \begin{bmatrix} X_1 \\ X_{2(i)} \end{bmatrix} = \begin{bmatrix} W_1 \\ R_{2(1)} + R_{2(2)} + \ldots + R_{2(i)} \end{bmatrix} \tag{9}$$

Therefore, the estimated parameters at the ith ($i > 1$) epoch can be expressed as follows:

$$\begin{bmatrix} X_1 \\ X_{2(i)} \end{bmatrix} = \begin{bmatrix} N_{11} & N_{12} \\ 0 & N_{2(1)} + N_{2(2)} + \ldots + N_{2(i)} \end{bmatrix}^{-1} \begin{bmatrix} W_1 \\ R_{2(1)} + R_{2(2)} + \ldots + R_{2(i)} \end{bmatrix} \tag{10}$$

As rank deficiency exists in this matrix, one receiver clock is used as the datum to eliminate the rank deficiency [22].

2.2. UPD Estimation and AR Strategies

The wide-lane (WL) and narrow-lane (NL) ambiguities are used to express the IF ambiguity. They can be expressed as follows [23–25]:

$$\overline{N}_{r,w}^s = \left(\frac{L_1}{\lambda_1} - \frac{L_2}{\lambda_2} - \frac{f_1 P_1 + f_2 P_2}{(f_1 + f_2)\lambda_w} \right) = N_{r,w}^s + b_{r,w} - b_w^s \tag{11}$$

$$\overline{N}_{r,n}^s = \frac{\lambda_{IF}(f_1 + f_2)\overline{N}_{r,IF}^s}{c} - \frac{f_2 N_{r,wl}^s}{(f_1 - f_2)} = N_{r,n}^s + b_{r,n} - b_n^s \tag{12}$$

where $N_{r,w}^s$ denotes integer WL ambiguity, and $\overline{N}_{r,n}^s$ and $N_{r,n}^s$ indicate float and integer NL ambiguity, respectively. λ_1 and λ_2 are carrier phase wavelengths at frequencies 1 and 2, respectively. λ_w is the WL wavelength, which can be expressed as $\lambda_w = \frac{c}{f_1 - f_2}$. $b_{r,w}$ and $b_{r,n}$ represent receiver WL and NL UPD, respectively, and b_w^s and b_n^s represent their counterparts for the satellite. By using observations from a network, the matrix form is used to express the UPD estimation [26]:

$$\begin{bmatrix} B_1 \\ B_2 \\ \vdots \\ B_n \end{bmatrix} = \begin{bmatrix} R_1 & S_1 \\ R_2 & S_2 \\ \vdots & \vdots \\ R_n & S_n \end{bmatrix} \cdot \begin{bmatrix} b_r \\ b^s \end{bmatrix} \tag{13}$$

where B_n is the sum of the UPD on the satellite and receiver end for the *n*-th observation. R_n and S_n are the UPD coefficients. Because the satellite and receiver UPD are simultaneously estimated, the rank deficiency is eliminated by selecting a satellite UPD as the datum.

With the high-precision UPD products, AR can be performed. In the AR process, the WL ambiguity is first fixed, followed by the NL ambiguity. The WL ambiguity is insensitive to measurement noise and stable by using multi-epoch smoothing due to its longer wavelength. In this study, for the WL AR, the Rounding method [27] is applied, while for the NL AR, both the least-square ambiguity decorrelation adjustment (LAMBDA) with a better success rate and the Rounding method with less computational time have been applied to estimate the ambiguity-fixed satellite clock offsets [28,29]. To simplify the operation and avoid high-dimensional problems, the Rounding method is used for NL AR in this contribution [30]. The IF ambiguity using Equation (12) can be recovered once both the WL and NL ambiguities of one observation are fixed. The parameter update is then conducted, which can be expressed as follows [27]:

$$X_1 = X_1 + Q_{12} Q_{22}^{-1} \Delta X_2 \tag{14}$$

where X_1 is the float ambiguity vector, Q_{12} represents the variance–covariance matrix for float and fixed parameters, Q_{22} is the variance–covariance matrix of the fixed ambiguities, and ΔX_2 is the difference between fixed and float ambiguities.

2.3. Data Processing Flowchart

To further explain the data processing of the BDS-3 ambiguity-fixed satellite clock offset estimation, the data processing flowchart is displayed in Figure 1. The observation data, Earth rotation parameters (ERPs), satellite and receiver antenna information files, satellite orbits, and station coordinates are first read for further processing. Afterwards, data preprocessing, such as cycle slip, and outlier detection are conducted, and the ambiguity-float satellite clock offset is estimated, with the float ambiguities and clock offsets obtained. Thereafter, by using the observation data, the WL UPDs are estimated from a station network. Then, the NL UPDs are also estimated. The epoch-wise mode is applied for estimating UPDs. Next, the undifferenced ambiguities are fixed by using the estimated UPD products on the satellite and receiver end. Finally, the clock offset is updated in ambiguity-fixed mode and outputted.
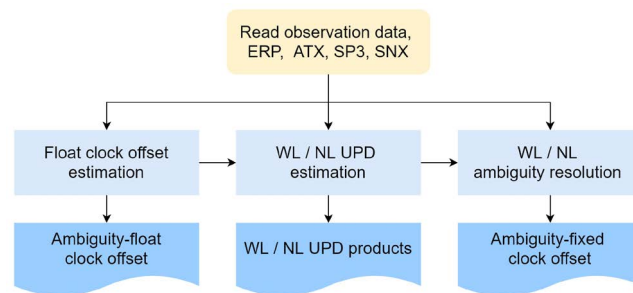
Figure 1. Data processing flowchart for ambiguity-fixed BDS-3 satellite clock offset estimation.

3. Experiment Analysis

In this section, the experimental setup is first introduced. Thereafter, the UPD performance, ambiguity fixing rate, clock offset accuracy, and PPP-AR are evaluated.

3.1. Experimental Setup

The BDS-3 ambiguity-fixed satellite clock offset with B1C/B2a and legacy B1I/B3I signals are estimated. In total, 85 globally distributed stations, from 18 June 2023 (day of the year (DOY) 169) to 24 June 2023 (DOY 175), were used for the processing, in which 8, 14, 45, and 18 stations were equipped with LEICA GR50, SEPT POLARX5TR, SEPT POLARX5, and TRIMBLE ALLOY receivers, respectively (see the red dots in Figure 2). DOY 169 is used to achieve convergence. The simulated real-time mode was applied for the experiment. The BDS-3 precise satellite orbits, the antenna PCO, and PCV released from Chang'an University were applied [10,31]. The International GNSS Service (IGS) weekly solutions were applied to fix the station coordinates. Four types of parameters were estimated, i.e., the satellite clock, the receiver clock, the ZWDs, and the phase ambiguities. The satellite and the receiver clock offsets are estimated as epoch-independent parameters. The Saastamoinen model is applied to calculate the zenith hydrostatic delay [32], and the ZWDs were estimated as piece-wise constants, updated on an hourly basis. The undifferenced IF ambiguities are fixed for each observation epoch-wise using the estimated WL and NL UPDs. Once the ambiguities are fixed, the clock offset can then be updated and outputted. Table 1 presents the detailed data processing strategies.

Table 1. Detailed data processing strategies.

Items	Strategies
Signal selection	B1C/B2a, B1I/B3I
Elevation mask	$7°$
Stochastic Model	1, *Elevation* > 30°; 2sin (*Elevation*), *Elevation* < 30°
Satellite orbit, PCO, and PCV	From Chang'an University [10,31]
ERP	IGS weekly solutions
Phase wind-up	Corrected [33]
Relativistic effects	Corrected [34]
Station coordinates	IGS weekly solutions applied
Clock offset estimator	Sequential least-squares adjustment [21]
UPD estimator	Kalman filter [30]
ZWD	Piece-wise constants and updated hourly
Phase ambiguities	Fixed to integers using the Rounding method for WL and NL ambiguities, epoch-wise
Satellite clock offset	White noise
Receiver clock offset	White noise
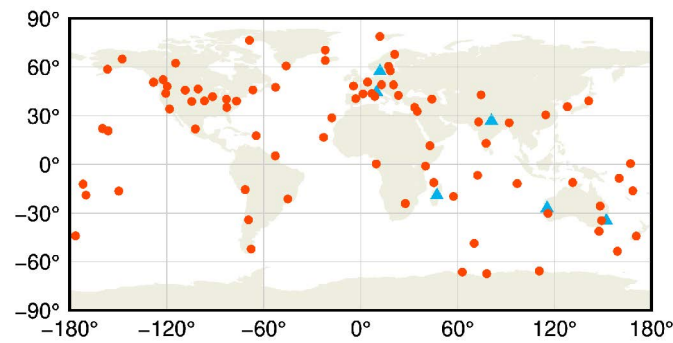
Figure 2. Station distribution for clock offset estimation (red dots) and PPP-AR (blue triangles).

3.2. UPD Performance

The integer characteristics of ambiguities are destroyed as the code and phase hardware delays are difficult to separate from the ambiguities. These delays should be precisely estimated before clock offset estimation. The UPD performance is the prerequisite for the undifferenced AR. Therefore, its performance is of great interest for this study. The satellite WL and NL UPDs of each epoch on DOY 172 for two signal combinations are displayed in Figure 3. In this figure, one satellite (C19) is selected as a reference. The satellite WL UPDs are remarkably stable for one day for both combinations, which is nearly constant within a day for each satellite. Compared to the WL UPDs, the larger fluctuations of the NL UPD time series can be observed. The largest fluctuation for B1I/B3I signals happened at C26 (0.678 cycles) and for B1C/B2a signals at C21 (0.530 cycles) on the test day.
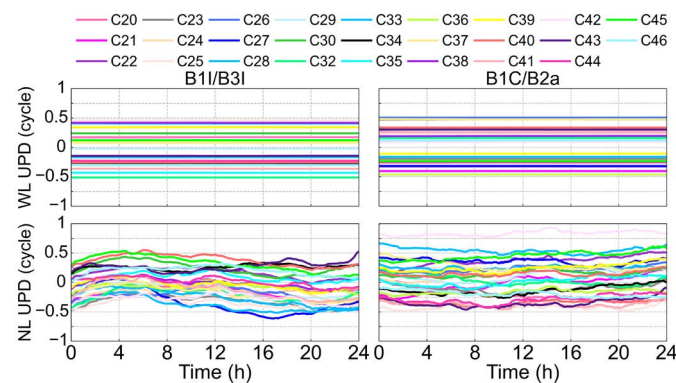
Figure 3. Satellite UPD time series on DOY 172, 2023, for two combined signals.

Figure 4 presents the standard deviations (STDs) of the daily mean satellite WL and NL UPDs. It can be observed that the stability of the WL UPDs is better when utilizing the B1I/B3I signal, while the STDs of the NL UPDs estimated using the B1C/B2a signals present better performance. The WL and NL wavelengths of B1I/B3I signals amount to 1.025 and 0.106 m, respectively, while they amount to 0.751 and 0.109 m for B1C/B2a signals, respectively. A larger wavelength implies less sensitivity of the integer ambiguity fixing to the measurement noise and mis-modeled effects. The mean STD of the NL UPDs is 0.122 cycles for B1I/B3I, and 0.081 cycles for B1C/B2a signals, showing better stability of the NL UPDs estimated from the B1C/B2a signals. Although the NL wavelength of these two signal combinations is nearly identical, the NL UPD stability using B1C/B2a is superior, which could be caused by its better observation quality [12,35]. Moreover, the STDs are larger on DOY 170 than on other days for both the WL and NL UPDs, which could be caused by the convergence problems during the initial processing time.
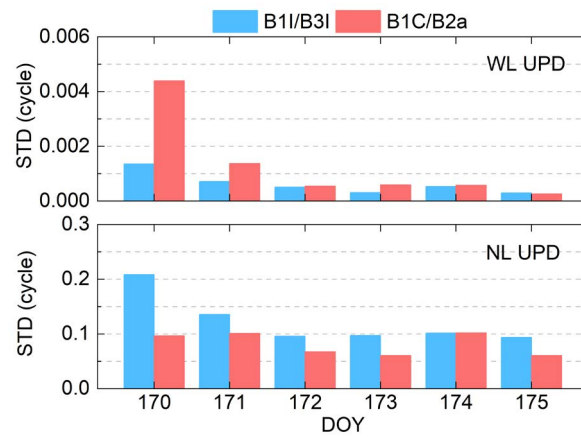
Figure 4. Daily STDs of the satellite WL and NL UPDs.

When performing undifferenced AR, the receiver UPD is also needed. The STDs of the UPDs on the receiver end are thus also assessed and shown in Figure 5. Except for Trimble alloy receivers, the WL UPD performance of the receiver shows similar performance for these two signal combinations. The STDs of the WL UPDs exhibit poor behaviors for Trimble alloy receivers when using the B1C/B2a signals, which may be related to its receiver hardware. For NL UPDs, the STDs calculated from these two signal combinations exhibit comparable performances. The mean STDs for the receiver WL UPDs are 0.004 cycles for B1I/B3I signals and 0.011 cycles for B1C/B2a signals, whereas the NL UPD stability are 0.131 cycles for B1I/B3I signals and 0.125 cycles for B1C/B2a signals.
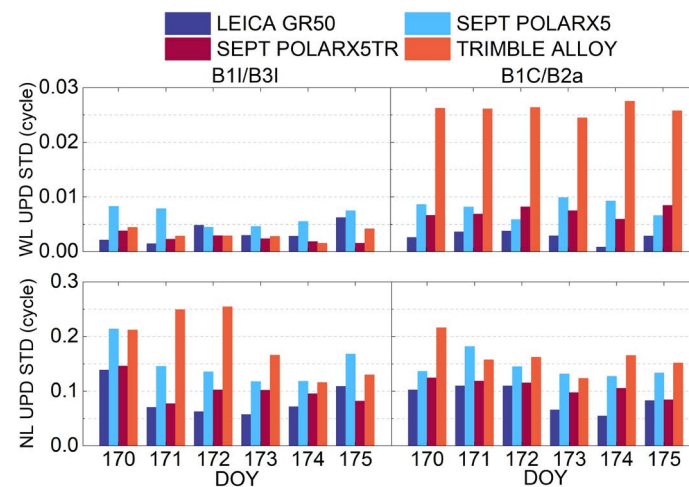
Figure 5. Daily STDs of the receiver WL and NL UPDs.

When the UPDs are removed from ambiguity, the ambiguity is near to an integer, and the difference between this value and the integer is regarded as the UPD residual [36], which is an indicator to check the estimated UPD quality. Figure 6 presents the daily UPD residual distribution percentages for both WL and NL and both frequency combinations. The WL UPD residual distribution of B1I/B3I signals is from 95.3% to 96.2% and 99.0% to 99.3% for (−0.25, 0.25) and (−0.15, 0.15) cycles, respectively, while for B1C/B2a signals, it is from 92.4% to 93.3% and from 98.0% to 98.6%, respectively. The distribution of WL UPD residuals for B1I/B3I signals is better due to its longer wavelength. Compared to B1I/B3I signals, the NL UPD residual distribution of the B1C/B2a signals is slightly better for both (−0.15, 0.15) and (−0.25, 0.25) cycles, which may be caused by the better observation quality of the B1C/B2a signals [12,35]. The NL UPD residual distribution shows better performance compared to that of the WL UPD.
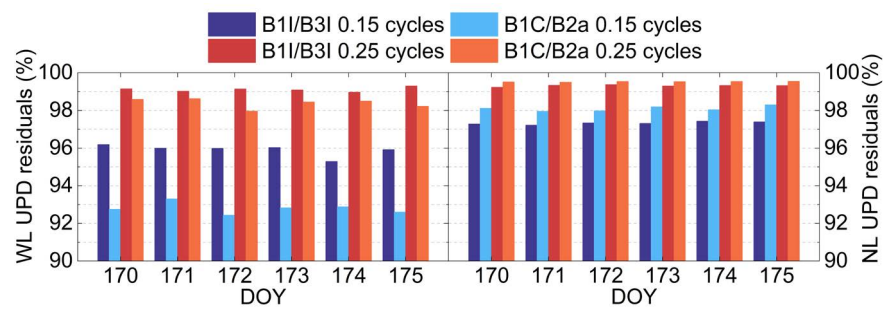
Figure 6. Daily UPD residual distribution percentages for B1I/B3I and B1C/B2a signals within (−0.15, 0.15) and (−0.25, 0.25) cycles.

3.3. Ambiguity Fixing Rate

After employing UPD products, when both the WL and NL ambiguity are less than 0.25 cycles, the ambiguity is regarded as fixed. The ambiguity fixing rate is that the ratio of the number of fixed NL ambiguities to the number of ambiguities. Figure 7 presents the ambiguity fixing rate of each epoch for these two signal combinations. After starting the procedure for about dozens of minutes, a high ambiguity fixing rate can be achieved due to the convergence process for high-precision UPD and ambiguities. After the convergence, the ambiguity fixing rate is between 70% and 90% for most epochs. The B1C/B2a signals exhibit a lower ambiguity fixing rate compared to the B1I/B3I signals. The WL wavelength of B1I/B3I is 1.025 m, and 0.751 m for B1C/B2a; the longer wavelength is beneficial to the WL AR. Furthermore, Figure 8 shows the number of raw observations for the two signal combinations at each epoch. It can be observed that there are more observations that can be applied for the B1I/B3I signal at most epochs, with the mean values amounting to 715 and 709, respectively. The model strength is decreased when reducing the number of observations. Moreover, the reduction phenomenon of the ambiguity fixing rate can be found at the day boundary for both signal combinations, which is caused by the satellite orbit discontinuity between adjacent days [37]. The mean ambiguity fixing rate of B1I/B3I and B1C/B2a signals is 80.7% and 78.0% from DOY 170 to 175, respectively. It can be observed from Figure 7 that the increasing speed of the ambiguity fixing rate at the beginning using B1C/B2a signals is faster compared to that of B1I/B3I signals; therefore, the performance of the ambiguity fixing rates is further investigated at the initialization phase. In Figure 9, the clock offset estimation is restarted every 8 h. The speed to reach an ambiguity fixing rate of 70% using B1C/B2a signals is significantly faster for all sessions. The mean time to first fix (TTFF) of these sessions is improved from 67.43 min using B1I/B3I signals to 23.74 min using B1C/B2a signals, with an improvement of 64.8%. The shorter TTFF is beneficial to a faster AR and a faster convergence of the satellite clock offset estimation. Figure 10 presents the mean Signal-to-Noise Ratio (SNR) of each frequency for each BDS-3 satellite at the GANP station on DOY 172, 2023. It can be seen that the SNR of B1I, B1C, and B3I are almost the same, while the SNR of B2a is better than those of other frequencies for most satellites. Moreover, the noise amplification factor of B1I/B3I and B1C/B2a is 3.528 and 2.588, respectively. The long convergence time of the B1I/B3I ambiguity fixing could be impacted by its observation data quality and larger noise amplification factor.
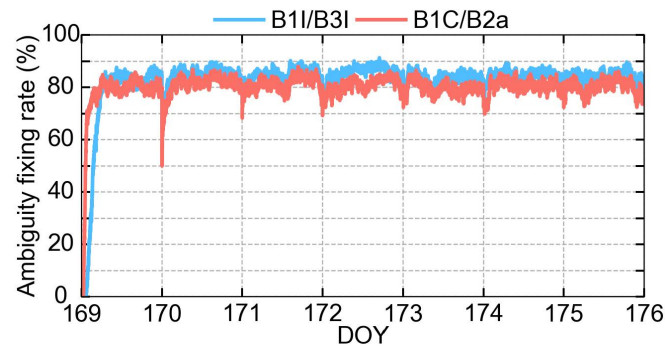
Figure 7. Epoch-wise ambiguity fixing rates for two combined signals (weekly solution).
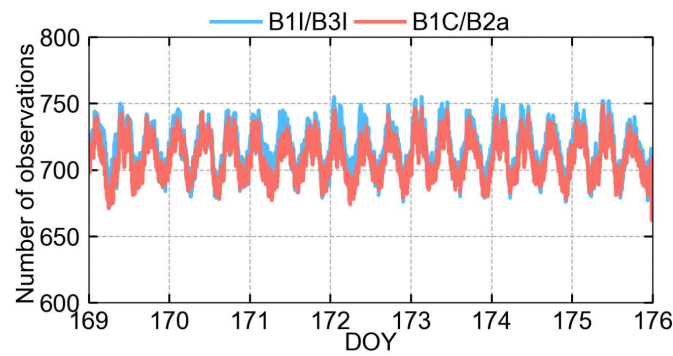
Figure 8. Number of observations for two combined signals at each epoch.
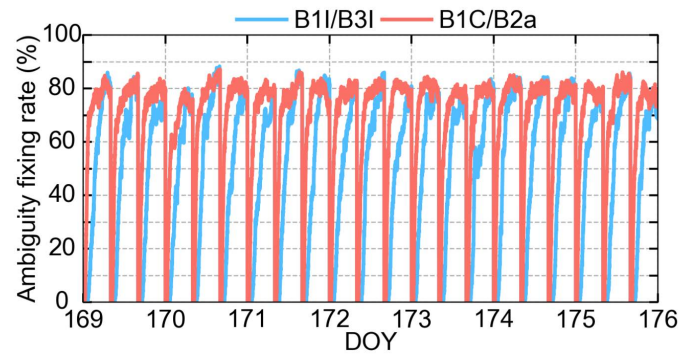
Figure 9. Epoch-wise ambiguity fixing rates for two signal combinations with the processing restarted every 8 h.
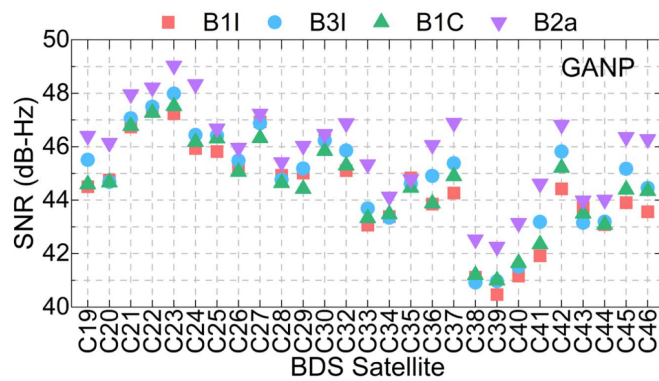
Figure 10. Mean SNR of each frequency for each BDS-3 satellite at GANP stations on DOY 172, 2023.

3.4. Clock Offset Accuracy

The satellite orbits are fixed when estimating the satellite clock offsets using different signal combinations. Therefore, we first analyze the satellite orbital consistency when using the two signal combinations. The BDS-3 satellite orbital difference in the three directions between the two signal combinations on DOY 172 is presented in Figure 11. The satellite orbit difference is between −5 and 5 cm for most BDS-3 MEO satellites, while larger fluctuations can be found for BDS-3 IGSO satellites (C38, C39, C40), showing worse performance due to their poorer geometries. Figure 12 presents the orbital accuracy for each BDS-3 satellite from DOY 169 to 175. The satellite orbital consistency is better than 2 cm for most MEO satellites in all three directions.
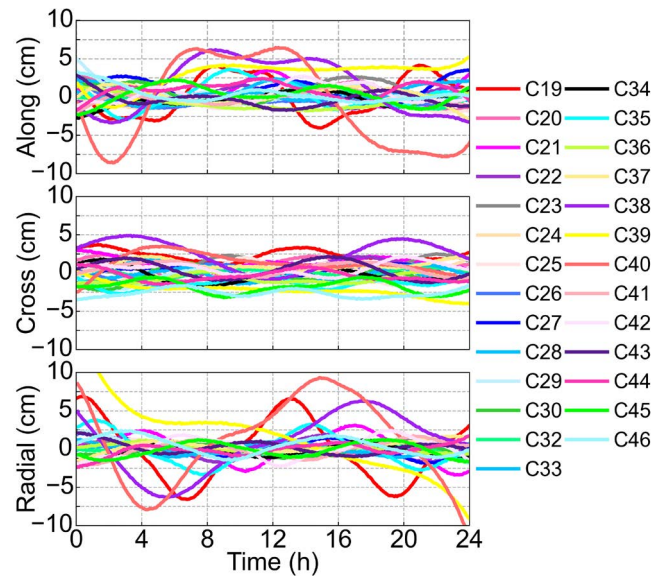
Figure 11. BDS-3 satellite orbital inconsistency between two signal combinations on DOY 172, 2023.
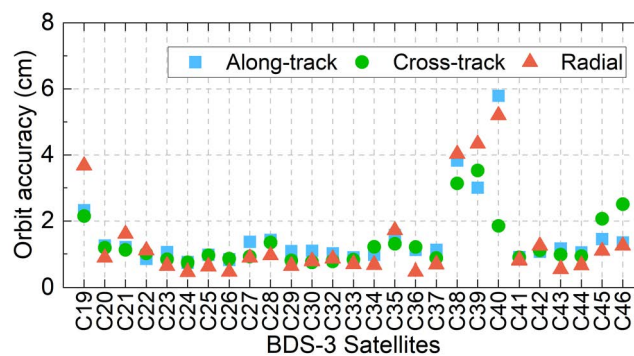
Figure 12. BDS-3 satellite orbital accuracy between the cases using two signal combinations.

The estimated clock offset accuracy is evaluated using the typical double-difference method [2]. The satellite clock offset products from Chang'an University are used as references. The ambiguity-float and -fixed satellite clock offset errors estimated from the two signal combinations on DOY 172 are shown in Figure 13. The clock errors fall within the range of −0.5 to 0.5 ns for both ambiguity-float and -fixed solutions using two signal combinations. After fixing ambiguities, the clock offset difference is better compared to the ambiguity-float case. The mean ambiguity-fixed clock precision (STD) on DOY 172 is 0.027 ns for B1I/B3I signals and 0.024 ns for B1C/B2a signals. Since the BDS satellite orbits were estimated on a daily basis, the day boundary discontinuities of satellite orbits exist between adjacent days [37]. Therefore, when using the satellite orbits from two adjacent days for interpolation, these discontinuities will result in some outliers at the end of the day.
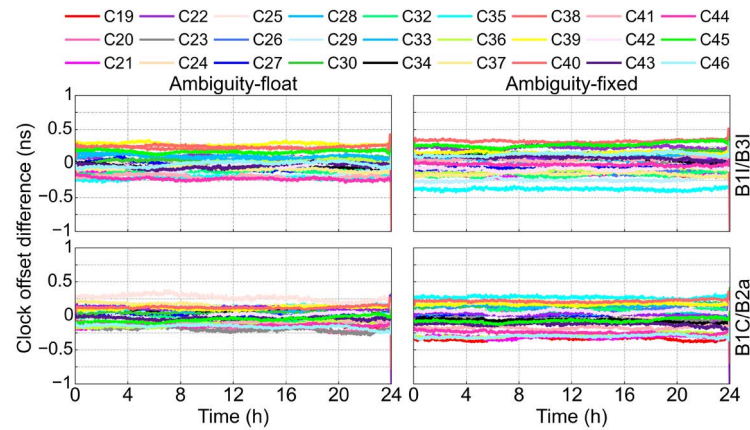
Figure 13. Ambiguity-float and -fixed satellite clock errors when using two combined signals on DOY 172.

Figure 14 presents the mean clock precision for each satellite of the two signal combinations. For the ambiguity-float solutions using B1I/B3I signals, the STD of the clock errors ranges from 0.022 to 0.052 ns, in which for satellites C27 and C38, the STDs are beyond 0.05 ns. For B1C/B2a signals, the STDs are better than 0.05 ns for all satellites, ranging from 0.020 to 0.048 ns. After fixing the ambiguities, the clock precision is improved for most satellites, whereas the largest improvements amount to 63.8% for C27 using B1I/B3I signals, and 34.5% for C22 using B1C/B2a signals. Moreover, except for C38, the precision difference among different satellites is small. The mean clock precision of the ambiguity-float is 0.033 ns using B1I/B3I signals and 0.024 ns using B1C/B2a signals. After fixing the ambiguities, they are improved to 0.026 and 0.023 ns using B1I/B3I and B1C/B2a signals, with corresponding improvements of 27.3% and 7.7%, respectively. Compared to clock offset estimation with B1I/B3I signals, the improvement when using B1C/B2a amounts to 21.2% for the ambiguity-float solutions, and 4.2% for ambiguity-fixed solutions. The improvements in satellite clock precision demonstrate better performance when using the B1C/B2a signals.
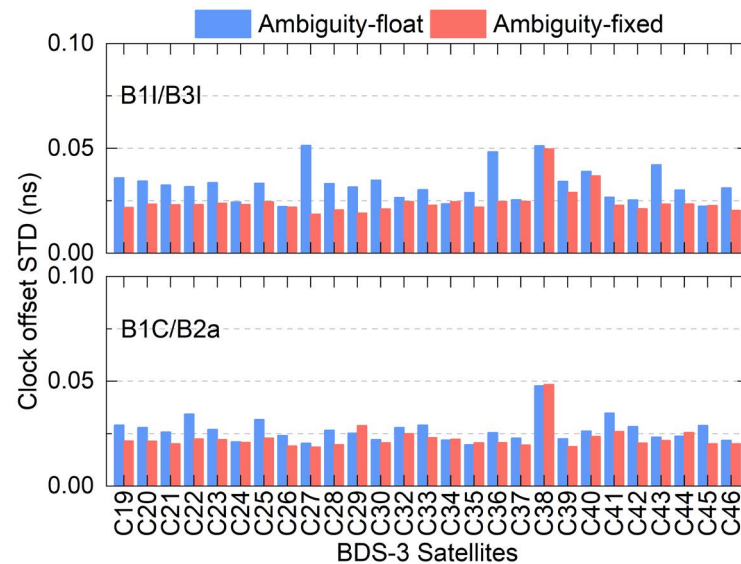
Figure 14. Mean BDS-3 satellite clock precision when using two combined signals in ambiguity-float and -fixed modes.

3.5. PPP Validation

PPP is an effective method to validate the estimated ambiguity-fixed satellite clock offsets. In this section, the kinematic PPP is performed in a BDS-3-only scenario to validate the performances of the estimated UPDs and ambiguity-fixed clock offsets. Six other stations different from those used for clock estimation were utilized for the PPP validation (see the blue triangles in Figure 2). Four schemes were tested, i.e., PPP and PPP-AR using the two signal combinations. The positioning errors on DOY 172 at a typical station, i.e., STR1, are illustrated in Figure 15. By applying the PPP-AR, the convergence time is significantly shortened, and the east component is more remarkable. After the convergence, the positioning errors are also more stable for the PPP-AR case. For the PPP-AR using two different signal combinations, the B1C/B2a signals can achieve faster convergence, possibly due to its better signal quality, smaller noise amplification factor and satellite orbital accuracy.
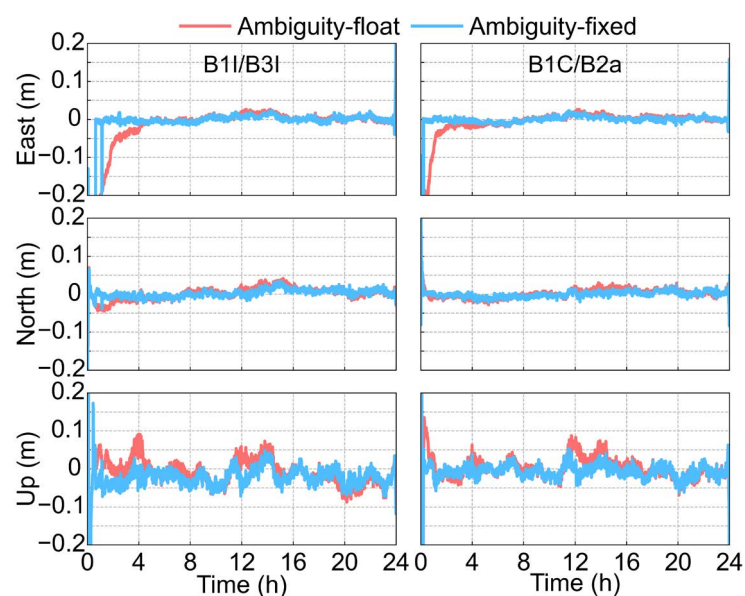
Figure 15. Positioning errors of the ambiguity-float and -fixed PPP using B1I/B3I and B1C/B2a signals for station STR1 on DOY 172, 2023.

Figure 16 shows the mean positioning accuracy of each station. It can be observed that the positioning accuracy when using PPP-AR is remarkably better than the ambiguity-float solutions, especially in the E direction [28]. Table 2 presents the mean positioning accuracy for different cases. The positioning accuracy is better than 3 cm, 2 cm, and 6 cm for the E, N, and U directions, respectively, in all cases. The positioning accuracy of ambiguity-float PPP amounts to 2.57, 1.64, and 5.16 cm for the E, N, and U components when using the B1I/B3I signals, respectively, and it is improved to 1.56, 1.23, and 4.46 cm after ambiguity-fixing, with improvements of 39.3%, 25.0%, and 13.6% in the three directions. In terms of the B1C/B2a signals, when using PPP-AR, the mean positioning accuracy is improved from 2.75 to 1.36 cm, 1.56 to 1.16 cm, and 5.04 to 4.25 cm for the E, N, and U components, with improvements of 50.6%, 25.6%, and 15.8%, respectively. The PPP-AR using B1C/B2a signals shows better performance for all three positional components. The improvement amounts to 12.8%, 5.7%, and 4.7% for the E, N, and U components, respectively. Moreover, we also investigate the convergence time of PPP and PPP-AR, which is another indicator to check the performance of PPP, its definition is that the elapsed time is needed to achieve a positioning accuracy better than 10 cm and to keep it within 10 min in three directions. Table 3 presents the convergence time. The convergence time can be shortened after using ambiguity-fixing for both signal combinations. The convergence time is shortened from 36.69, 13.70, and 31.43 min when using the ambiguity-fixed clock from B1I/B3I signals to

23.79, 12.33, and 20.98 min when using B1C/B2a signals, with improvements of 35.2%, 10.0%, and 33.3% in the E, N, and U directions, respectively.
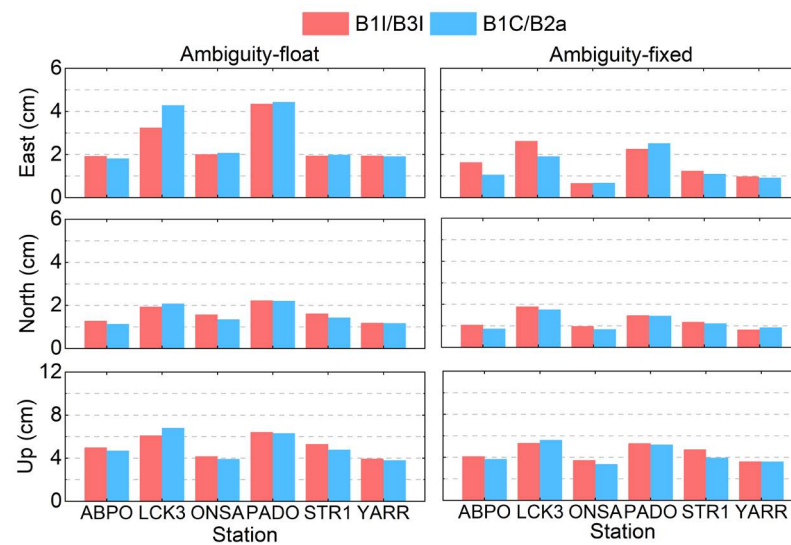
Figure 16. Mean positioning accuracy for the six test stations.

Table 2. Mean positioning accuracy of all stations (unit: cm).

	B1I/B3I Float	B1C/B2a Float	B1I/B3I Fixed	B1C/B2a Fixed
East	2.57	2.75	1.56	1.36
North	1.64	1.56	1.23	1.16
Up	5.16	5.05	4.46	4.25

Table 3. Mean convergence time of all stations (unit: min).

	B1I/B3I Float	B1C/B2a Float	B1I/B3I Fixed	B1C/B2a Fixed
East	66.57	39.45	36.69	23.79
North	13.73	12.95	13.70	12.33
Up	42.93	37.25	31.43	20.98

4. Discussion

In the current BDS-3, more signal combinations can be selected by users. It has been reported that the B1C/B2a has better signal strength because of the longer bandwidth of the Asymmetric Constant Envelope BOC (ACE-BOC) modulation, and a smaller noise amplification factor compared to that of the B1I/B3I signal combination [38]. While the BDS-3 satellite clock offsets are currently often estimated using B1I/B3I signals in many analysis centers, this contribution investigates the BDS-3 satellite clock offset in real-time with AR using the new B1C/B2a signal combination. The results showed that the performances of the TTFF, the satellite clock precision, and kinematic PPP-AR results using B1C/B2a signals are all better than those using the B1I/B3I signals, which suggests it should be used in more future applications. It can be anticipated that the B1C/B2a observations can be used to generate BDS-3 real-time satellite clocks from various analysis centers in the near future, which can then be applied to BDS-related applications.

5. Conclusions

The BDS-3 can transmit on five frequencies. It has been proven that AR can improve the performance of precise data processing. This contribution investigates the ambiguity-fixed BDS-3 real-time satellite clock offset using new B1C/B2a signals; the ambiguity-float satellite clock estimation, the UPD estimation, and the AR are conducted sequentially.

The estimated ambiguity-fixed satellite clock offset is evaluated from the following aspects: the UPD performance, the ambiguity fixing rate, the satellite clock precision, and the positioning accuracy. The satellite WL UPDs estimated from the two signal combinations are stable, while the NL UPD stability for B1C/B2a signals is better. The WL UPD residual distribution for B1I/B3I signals is superior due to its larger wavelength, whereas the NL UPD residual distribution estimated from B1C/B2a shows better performance. For B1I/B3I and B1C/B2a signals, the mean ambiguity fixing rate amounts to 80.7% and 78.0%, respectively. The TTFF of the ambiguity fixing rates for B1C/B2a signals is significantly shorter than that of B1I/B3I signals. The clock offset precision of the ambiguity-float and -fixed scenarios are 0.033 and 0.026 ns for the B1I/B3I signal combination, respectively, while it amounts to 0.024 and 0.023 ns for B1C/B2a signals, respectively. The positioning performance of PPP-AR is 1.56, 1.23, and 4.46 cm in the E, N, and U directions for B1I/B3I signals, respectively, while it amounts to 1.36, 1.16, and 4.25 cm for B1C/B2a signals. When using the satellite clock offsets from B1C/B2a signals to conduct PPP-AR, the convergence time is shorter. All results have demonstrated that the estimated clock offset using BDS-3 and new B1C/B2a signals is better.

The PPP-AR results obtained in this study are based on kinematic coordinate estimation using static stations, which mainly apply to scenarios in open-sky areas. In real kinematic experiments in suburban or urban areas, the processing suffers from higher multipath effects that degrade the AR performances and the positioning accuracy using the B1C/B2a signals. This awaits further study in the future.

Author Contributions: W.X. proposed the methodology, conducted the experiments, prepared figures, and wrote the manuscript. W.F. developed the methodology and reviewed the manuscript. S.X. conducted the experiments and reviewed the manuscript. K.W., B.C. and M.L. reviewed the manuscript. All authors contributed to the writing of this manuscript. All authors have read and agreed to the published version of the manuscript.

Conflicts of Interest: The authors declare no conflicts of interest.

References

1. Yang, Y.; Gao, W.; Guo, S.; Mao, Y.; Yang, Y. Introduction to BeiDou-3 navigation satellite system. *Navigation* **2019**, *66*, 7–18. [CrossRef]
2. Huang, G.; Cui, B.; Zhang, Q.; Fu, W.; Li, P. An improved predicted model for BDS ultra-rapid satellite clock offsets. *Remote Sens.* **2018**, *10*, 60. [CrossRef]
3. Xie, W.; Huang, G.; Fu, W.; Shu, B.; Cui, B.; Li, M.; Yue, F. A quality control method based on improved IQR for estimating multi-GNSS real-time satellite clock offset. *Measurement* **2022**, *201*, 111695. [CrossRef]
4. CSNO. *BeiDou Navigation Satellite System Signal in Space Interface Control Document Open Service Signal B1I (Version 3.0)*; China Satellite Navigation Office: Beijing, China, 2019.
5. CSNO. *BeiDou Navigation Satellite System Signal in Space Interface Control Document Open Service Signal B3I (Version 1.0)*; China Satellite Navigation Office: Beijing, China, 2018.

6. CSNO. *BeiDou Navigation Satellite System Signal in Space Interface Control Document Open Service Signal B1C (Version 1.0)*; China Satellite Navigation Office: Beijing, China, 2017.

7. CSNO. *BeiDou Navigation Satellite System Signal in Space Interface Control Document Open Service Signal B2a (Version 1.0)*; China Satellite Navigation Office: Beijing, China, 2017.

8. Lu, M.; Li, W.; Yao, Z.; Cui, X. Overview of BDS III new signals. *Navigation* **2019**, *66*, 19–35. [CrossRef]

9. He, L.; He, X.; Huang, Y. Enhanced precise orbit determination of BDS-3 MEO satellites based on ambiguity resolution with B1C/B2a dual-frequency combination. *Measurement* **2022**, *205*, 112197. [CrossRef]

10. Xie, S.; Huang, G.; Wang, L.; Yan, X.; Qin, Z. Estimation of Vertical Phase Center Offset and Phase Center Variations for BDS-3 B1CB2a Signals. *Remote Sens.* **2022**, *14*, 6380. [CrossRef]

11. Kuang, K.; Wang, J.; Han, H. Real-Time BDS-3 Clock Estimation with a Multi-Frequency Uncombined Model including New B1C/B2a Signals. *Remote Sens.* **2022**, *14*, 966. [CrossRef]

12. Zhang, Q.; Zhu, Y.; Chen, Z. An In-Depth Assessment of the New BDS-3 B1C and B2a Signals. *Remote Sens.* **2021**, *13*, 788. [CrossRef]

13. Li, M.; Mu, R.; Jiang, K.; Wang, Y.; Zhang, X.; Chang, C.; Zhao, Q. Precise orbit determination for the Haiyang-2D satellite using new onboard BDS-3 B1C/B2a signal measurements. *GPS Solut.* **2022**, *26*, 137. [CrossRef]

14. Zhao, L.; Hua, X.; Tang, X.; Cao, Y.; Zhou, S.; Yang, Y.; Liu, L.; Guo, R. Generation of DFMC SBAS corrections for BDS-3 satellites and improved positioning performances. *Adv. Space Res.* **2020**, *66*, 702–714. [CrossRef]

15. Hou, Y.; Wang, H.; Wang, J.; Ma, H.; Ren, Y.; Liu, Y. BDS-3 new signals observable-specific phase biases estimation and PPP ambiguity resolution. *Adv. Space Res.* **2023**, *72*, 2156–2169. [CrossRef]

16. Yu, X.; Cao, X.; Wang, J.; Ge, Y.; Shen, F. The benefit of B1C/B2a signals for BDS-3 wide-area decimeter-level and centimeter-level point positioning with observable-specific signal bias. *Measurement* **2023**, *214*, 112815. [CrossRef]

17. Ren, Z.; Gong, H.; Lyu, D.; Peng, J.; Guo, Y.; Sun, G. Time transfer with BDS-3 signals: CV, PPP and IPPP. *Meas. Sci. Technol.* **2023**, *34*, 045007. [CrossRef]

18. Li, X.; Xiong, Y.; Yuan, Y.; Wu, J.; Li, X.; Zhang, K.; Huang, J. Real-time estimation of multi-GNSS integer recovery clock with undifferenced ambiguity resolution. *J. Geod.* **2019**, *93*, 2515–2528. [CrossRef]

19. Montenbruck, O.; Steigenberger, P.; Prange, L.; Deng, Z.; Zhao, Q.; Perosanz, F.; Romero, I.; Noll, C.; Stürze, A.; Weber, G.; et al. The multi-GNSS experiment (MGEX) of the international GNSS Service (IGS)—Achievements, prospects and challenges. *Adv. Space Res.* **2017**, *59*, 1671–1697. [CrossRef]

20. Li, X.; Li, X.; Liu, G.; Feng, G.; Guo, F.; Yuan, Y.; Zhang, K. Spatial-temporal characteristic of BDS phase delays and PPP ambiguity resolution with GEO/IGSO/MEO satellites. *GPS Solut.* **2018**, *22*, 123. [CrossRef]

21. Fu, W.; Yang, Y.; Zhang, Q.; Huang, G. Real-time estimation of BDS/GPS high-rate satellite clock offsets using sequential least squares. *Adv. Space Res.* **2018**, *62*, 477–487. [CrossRef]

22. Xie, W.; Huang, G.; Fu, W.; Li, P.; Cui, B. An efficient clock offset datum switching compensation method for BDS real-time satellite clock offset estimation. *Adv. Space Res.* **2021**, *68*, 1802–1813. [CrossRef]

23. Hatch, R. The synergism of GPS code and carrier measurements. In Proceedings of the Third International Symposium on Satellite Doppler Positioning at Physical Sciences Laboratory of New Mexico State University, Las Cruces, Mexico, 8–12 February 1982; Volume 2, pp. 1213–1231.

24. Melbourne, W.G. The case for ranging in GPS-based geodetic systems. In Proceedings of the First International Symposium on Precise Positioning with the Global Positioning System, Rockville, MD, USA, 15–19 April 1985; pp. 5–19.

25. Wübbena, G. Software developments for geodetic positioning with GPS using TI-4100 code and carrier measurements. In Proceedings of the First International Symposium on Precise Positioning with the Global Positioning System, Rockville, MD, USA, 15–19 April 1985; pp. 5–19.

26. Cui, B.; Li, P.; Wang, J.; Ge, M.; Harald, S. Calibrating receiver-type-dependent wide-lane uncalibrated phase delay biases for PPP integer ambiguity resolution. *J. Geod.* **2021**, *95*, 82. [CrossRef]

27. Dong, D.; Bock, Y. Global positioning system network analysis with phase ambiguity resolution applied to crustal deformation studies in California. *J. Geophys. Res.* **1989**, *94*, 3949–3966. [CrossRef]

28. Xie, W.; Huang, G.; Fu, W.; Li, M.; Du, S.; Tan, Y. Realizing rapid re-convergence in multi-GNSS real-time satellite clock offset estimation with dual-thread integer ambiguity resolution. *GPS Solut.* **2023**, *27*, 54. [CrossRef]

29. Liu, S.; Yuan, Y. Generating GPS decoupled clock products for precise point positioning with ambiguity resolution. *J. Geod.* **2022**, *96*, 6. [CrossRef]

30. Fu, W.; Wang, J.; Wang, L.; Chen, R. A Kalman filter-based online fractional cycle bias determination method for real-time ambiguity-fixing GPS satellite clock estimation. *Measurement* **2022**, *205*, 112207. [CrossRef]

31. Yan, X.; Liu, C.; Huang, G.; Zhang, Q.; Wang, L.; Qin, Z.; Xie, S. A Priori Solar Radiation Pressure Model for BeiDou-3 MEO Satellites. *Remote Sens.* **2019**, *11*, 1605. [CrossRef]

32. Saastamoinen, J. Contributions to the theory of atmospheric refraction—Part II. Refraction corrections in satellite geodesy. *Bull. Géodésiqu* **1973**, *47*, 13–34. [CrossRef]

33. Wu, J.T.; Wu, S.C.; Hajj, G.A.; Bertiger, W.I.; Lichten, S.M. Effects of antenna orientation on GPS carrier phase. In Proceedings of the Astrodynamics 1991, San Diego, CA, USA, 19–22 August 1991; pp. 1647–1660.

34. Kouba, J. Relativity effects of Galileo passive hydrogen maser satellite clocks. *GPS Solut.* **2019**, *23*, 117. [CrossRef]

35. Li, M.; Huang, G.; Wang, L.; Xie, W.; Yue, F. Performance of Multi-GNSS in the Asia-Pacific Region: Signal Quality, Broadcast Ephemeris and Precise Point Positioning (PPP). *Remote Sens.* **2022**, *14*, 3028. [CrossRef]
36. Li, X.; Liu, G.; Li, X.; Zhou, F.; Feng, G.; Yuan, Y.; Zhang, K. Galileo PPP rapid ambiguity resolution with five-frequency Observations. *GPS Solut.* **2020**, *24*, 24. [CrossRef]
37. Griffiths, J.; Ray, J.R. On the precision and accuracy of IGS orbits. *J. Geod.* **2009**, *83*, 277–287. [CrossRef]
38. Yao, Z.; Zhang, J.; Lu, M. ACE-BOC: Dual-frequency constant envelope multiplexing for satellite navigation. *IEEE Trans. Aerosp. Electron. Syst.* **2016**, *52*, 466–485. [CrossRef]